Chapter 4
Core/Shell Bimagnetic Nanoparticles

Elin L. Winkler and Roberto D. Zysler

Abstract The advances in the physical and chemical fabrication methods have enabled the possibility to produce artificial nanostructures whose properties are different from that of their constituent materials. The presence of interfaces in core/shell bimagnetic nanoparticles introduces additional interactions that could radically modify the static and dynamic magnetic behavior of the systems. The number of parameters that governs the magnetic behavior grows enormously and the opportunity to manipulate, control, and understand the role played by each one of them, opens a wide range of possibilities to design novel materials with suited properties. The magnetic response changes depend on the magnetic ordering and anisotropy of the phases, the core size and shell thickness, the quality of the interface, and the strength of the interface exchange coupling. In this chapter, we discuss the new properties found in core/shell bimagnetic nanoparticles and analyze the main characteristics that have to be taken into account to design a system with a particular response.

4.1 Introduction

The magnetism has had a tremendous impact on our daily life, and it has transformed our society, the way we see the world and the way we communicate each other. These days, it exist a huge demand of new materials to be used in numerous applications, and for developing new smaller devices and with improved performance. Large part of

E. L. Winkler (✉) · R. D. Zysler (✉)
Centro Atómico Bariloche and Instituto Balseiro Comisión Nacional de Energía Atómica (CNEA), Consejo Nacional de Investigaciones Científicas Y Técnicas (CONICET), Universidad Nacional de Cuyo (UNCUYO), Av. E. Bustillo 9500, R8402AGP San Carlos de Bariloche, Río Negro, Argentina
e-mail: winkler@cab.cnea.gov.ar

R. D. Zysler
e-mail: zysler@cab.cnea.gov.ar

D. Peddis et al. (eds.), *New Trends in Nanoparticle Magnetism*,
Springer Series in Materials Science 308,
https://doi.org/10.1007/978-3-030-60473-8_4

the research on field was driven by looking for harder and softer magnetic materials, and compounds for magnetic recording.

One important area in this field is the development of high-performance permanent magnets which requires hard magnetic materials with large energy product $(BH)_{max}$. Most of the progress in this area was reached from the design of new alloys that combines 3d ions coupled with rare-earth ions as $SmCo_5$, $Nd_2Fe_{14}B$, $Sm_2Fe_{17}N_3$, in this way compounds with large remanent magnetization and large coercive field are obtained. Novel ways to fabricate permanent magnets exploit the exchange length of the magnetic materials by combining at nanoscale soft with hard magnetic materials, composites with large magnetization, and also large magnetic anisotropy could be obtained. This strategy also opens new possibilities to fabricate new compounds with large energy products and rare-earth free magnets which would lower the cost of raw materials for manufacturing, and also simplify production due to the limitations of obtaining rare earth. The dimension of each component is determinant in this family of nanostructures and as a consequence fine control of the morphology and structure at nanoscale is mandatory.

The miniaturization of the magnetic devices and the increasing demand of high-density data storage materials also have driven the research in material science. The pushing toward high-density data storage in smaller dimensions has to face the well-known superparamagnetic limits so other approaches based on exchange coupling bimagnetic materials at nanoscale emerge as a possible solution. As it was mentioned previously, the current strategy does not go through the search for new compounds, although it cannot be ruled out to find a new phase with astonishing properties, but it is looking to design and manufacture new compounds from the possibility of manipulating and combining materials at the nanoscale. New synthesis and physical fabrication methods give a huge impulse to the area. The possibility of combining in a single nanoparticle two or more components, with controlled size and high quality of interfaces, opens a wide range of new possibilities.

The presence of interfaces in core/shell bimagnetic nanoparticles introduces additional interactions that could radically modify the static and dynamic magnetic behavior of the systems. The number of parameters that governs the magnetic behavior grows enormously and the opportunity to manipulate, control, and understand the role playing by each one of them opens a wide range of possibility to design novel materials with suited properties. The magnetic response changes depend on the magnetic ordering and anisotropy of the phases, the core size and shell thickness, the quality of the interface, and the strength of the interface exchange coupling. As a consequence, different behaviors named exchange spring, exchange bias, magnetic hardening, and proximity effects are observed. In this chapter, we are going to focus on the advances reached in the fabrication and the new properties found in core/shell bimagnetic nanoparticles, and we will discuss the main characteristics that have to be taken into account to design a particular system. The chapter is organized as follows: in Sect. 4.2, a brief summary of the most used synthesis methods is given. In Sect. 4.3, we will focus on the phenomenology and the physical parameters that determine the magnetic response of the core/shell system. In Sect. 4.4, we are going to present a case study, CoO-core/$Co_{1-x}Zn_xFe_2O_4$-shell nanoparticles with $x = 0$–1,

where the tuning of the coercive field, the thermal stability and the exchange bias will be attained by controlling the size and the interface exchange coupling. Finally, in the last section, future perspectives on the field will be described.

4.2 Synthesis and Production of Core/Shell Nanoparticles

The advances in the chemical and physical fabrication methods have enabled a continuous production of novel multifunctional nanostructures. In the particular case of bimagnetic nanoparticles, according to the technological challenge or basic research, different core/shell structures, including FM(FiM)-core/AFM-shell [1, 5, 9], FM-core/FiM-shell [66], hard/soft FiM-core/FiM-shell [11, 39], inverted AFMcore/FiM-shell [30, 36], doubly inverted AFM-core/FiM-shell ($T_N > T_C$) [53], and multishell nanoparticles [54], have been fabricated.

A physical approach to the fabrication of bimagnetic nanoparticles is based on obtaining the initial nanoparticles by known methods as gas condensation, thermal plasma, or spray pyrolysis. These initial particles can be formed, in general, by simple metals, alloys, or oxides. A second step, consisting of a post-treatment of partial reduction of oxides or oxidation of alloys (or overoxidation of certain oxides), provides a core/shell architecture to the nanoparticles. An example of oxidation of metallic particles has been reported in the initial paper of the exchange bias phenomena where cobalt particles were oxidized giving a Co/CoO ferromagnetic/antiferromagnetic core/shell structure [43]. Another example of oxidation of seeded nanoparticles is given by the Ni/NiO (ferromagnetic/antiferromagnetic) core/shell structures [23]. On the other hand, the reduction of transition metal oxides by annealing in reducing atmosphere (e.g., H_2) can also be used to obtain the desired core/shell nanostructures as the CoO (Co_3O_4)/Co antiferromagnetic/ferromagnetic inverted core/shell structure [63] or $CoFe_2O_4/CoFe_2$ [20].

The concept to produce core/shell nanoparticles by chemical route is similar. Single-phase nanoparticles are synthesized by a particular chemical method, and using the same concept of superficial post-treatment, an oxidation (reduction) is taking effect in order to obtain the core/shell structure. Many chemical routes give high control of composition, crystallinity, and size. There exists a large diversity of synthesis methods such as co-precipitation [13], sol–gel [64], cation exchange process [59], and thermal decomposition [35, 45]. Although it is very simple to obtain core/shell architecture by post-processing the surface, there are inherent drawbacks to the method that limit its application, i.e., it is very difficult to control independently the core and shell sizes, and the shell composition is determined (and limited) by the core composition. On the other hand, these manufacturing methods produce a low quality of the core/shell interface. The last point is a major problem in the observation of the exchange bias effect and/or the enhancement of the coercive field.

Another interesting approach is the seed-mediated growth method. This procedure consists in the synthesis of the core and shell in two stages which enable to control independently both composition and size of each component This opens up many

possibilities for manufacturing new systems, where proper materials can be chosen to optimize the exchange interaction between the two magnetic phases, i.e., by minimizing the crystalline mismatch, selecting compounds with particular magnetization and magnetic anisotropy, etc. The seed-mediated high-temperature thermal decomposition method has shown high efficiency in producing monodispersed nanoparticles with high quality of crystalline order and well-defined interfaces. These characteristics make it one of the most used methods which enabled the fabrication of many novel core/shell bimagnetic nanoparticles, e.g., $CoO/CoFe_2O_4$ [36], $CoO/NiFe_2O_4$ [31], $CoFe_2O_4/MnFe_2O_4$ [57], $Fe_3O_4/\gamma\text{-}Mn_2O_3$ [24], $ZnFe_2O_4/CoFe_2O_4$ [42]. Also, two-step co-precipitation methods have proven to be appropriate for creating core/shell architecture. Examples of that are $\gamma\text{-}Fe_2O_3/CoO$ [55], SmCo/Co [65], and $CoFe_2O_4/Fe_3O_4$ [16]. The mentioned chemical routes, among many others [15], show an enormous versatility and easy to produce a great variety of bimagnetic core/shell nanoparticles, which make this field promising for the design and fabrication of new systems for fundamental studies or for the development of nanoparticles for a wide range of applications.

4.3 Interface Coupling Phenomenology and Models

As the size of a magnetic material is reduced to nanometric scale, the surface-to-volume ratio increases and, as a consequence, the surface effects became more relevant. For example, approximately 1% of the atoms are located at the surface of single-phase nanoparticles of 100 nm, while the proportion increases over the 60% when the size diminishes to 3 nm. Surface defects, broken bonds, variation in the interatomic distance and surface local anisotropy induce magnetic disorder and magnetic frustration. In bimagnetic core/shell nanoparticles, besides the surface effects, the presence of the interface between the two magnetically ordered phases introduces additional interactions that could radically modify the static and dynamic magnetic behavior of the systems. This interface interaction can generate a new behavior that is not present in any of the original components as exchange bias effect, exchange spring, and anisotropy enhancement, which present characteristic hysteresis loops as illustrated in Fig. 4.1. There are good and complete reviews in the literature that discuss in detail the models that describe these effects [14, 22, 25, 39, 46, 48], below we are going to mention the main characteristics that has to be taken into account to predict the behavior and for designing a particular system.

4.3.1 Exchange Bias Effect

In bimagnetic nanostructures with FM/AFM interfaces, the exchange bias effect (E_B) is typically manifested by a field shift (H_{EB}) of the hysteresis loop when the material is field cooled from temperatures higher than the Néel temperature of the AFM (T_N)

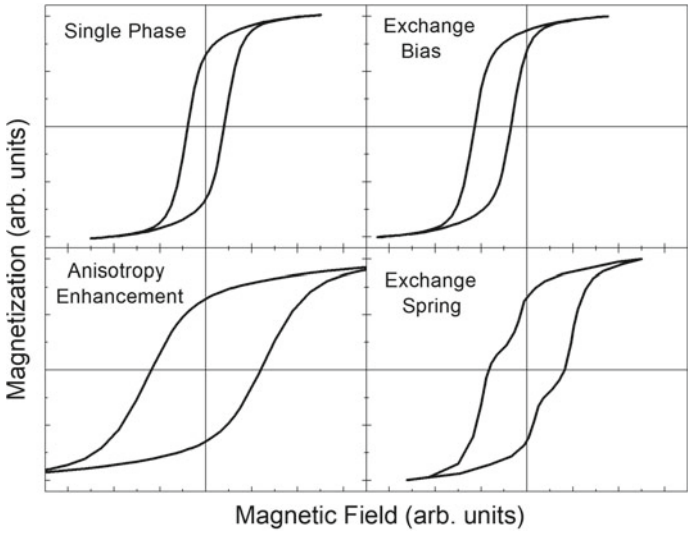

Fig. 4.1 Scheme of the magnetization loops for a single-phase magnetic nanoparticles and for different exchange coupled systems where exchange bias, anisotropy enhancement, and exchange spring behaviors are illustrated

and lower than the Curie temperature of the FM (T_C). The phenomenon is also related to other features as unidirectional anisotropy, coercive field enhancement, enhancement of the thermal stability of the nanoparticle magnetic moment, and vertical shift or asymmetric of the magnetization loop. Since the first observation of the unidirectional anisotropy in Co/CoO nanoparticles by Meilklejhon and Bean in 1956 [43], important advances have been made, both in the fabrication of new exchange bias structure and also in the development of theories explaining the origin of the observed behavior. Initially, most of the studies were made in thin films due to the high degree of control in the fabrication process, and they were impulsed by the crucial role played by the interfaces in technological application as read-head, high-density magnetic memories, spin valves, etc. Later, novel chemical route allowed a great control of the growing parameters of magnetic nanoparticles making it possible the design and fabrication of an enormous variety of biphase or even multiphase nanoparticles.

The physical origin of EB is usually explained by describing the pinning action exerted by the AFM over the FM(FiM) spins, as a consequence of the exchange coupling at the AFM/FM(FiM) interface. This interaction induces an extra torque to the magnetization reversal process and, depending to the ratio between the interface coupling energy and the anisotropy energy of the AFM, an asymmetry of the magnetization loops or enhancement of the coercive field, or both effects are observed. In a simple phenomenological model, considering the Zeeman interaction, the magnetic anisotropy of both phases, and the FM/AFM exchange interaction, the free energy of a FM/AFM coupled system can be expressed as:

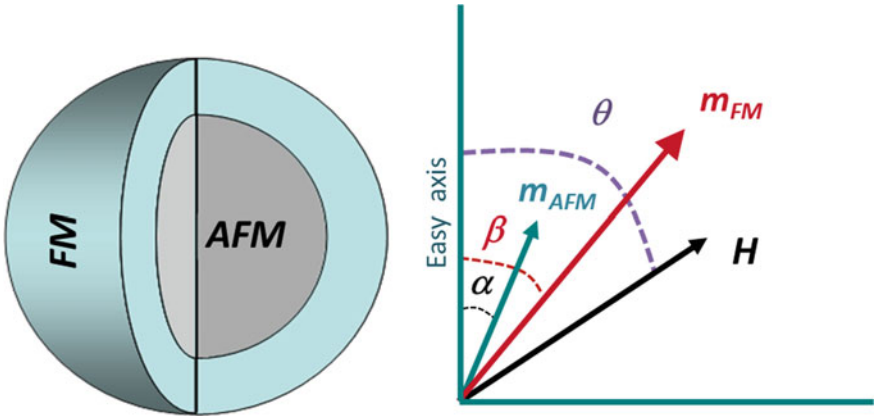

Fig. 4.2 Schematic representation of the magnetizations of the antiferromagnetic (m_{AFM}) and the ferromagnetic (m_{FM}) component of a core/shell nanoparticle, the magnetic field (H), and the angles involved in the description of the free energy

$$E = -Hm_{FM}V_{FM}.\cos(\theta - \beta) - Hm_{AFM}V_{AFM}\cos(\theta - \alpha) + K_{FM}V_{FM}\sin^2\beta + K_{AFM}V_{AFM}\sin^2\alpha - J_{EX}\cos(\beta - \alpha)$$

where H is the applied magnetic field, m_{FM} is the saturating FM magnetization normalized by the total FM volume (V_{FM}), m_{AFM} is the uncompensated AFM magnetization normalized by the total AFM volume (V_{AFM}), K_{FM} and K_{AFM} are the magnetic anisotropy of the FM and AFM phases, J_{EX} is the exchange coupling constant at the interface; the α, β, and θ are the angles between m_{AFM}, m_{FM}, and H with the easy axis direction, respectively, as shown in Fig. 4.2. The expression above includes two important approximations, the first one assumes a coherent rotation of the saturation magnetization with the field, and the second one assumes that the FM and AFM anisotropy easy axis are parallel.

From the above expression, two limit situations can be considered: $K_{AFM}V_{AFM} \gg J_{EX}$ and $K_{AFM}V_{AFM} \ll J_{EX}$. In the first case, $K_{AFM}V_{AFM} \gg J_{EX}$, after a field cooling process from a temperature $T_N < T < T_C$, the spins at the AFM interface align parallel (or antiparallel for $J_{EX} < 0$) to the FM phase in order to minimize the energy due to the interface exchange coupling. In this particular configuration, for $J_{EX} > 0$, the requested field to produce the inversion of the magnetization is higher in the opposite direction of the applied magnetic field which originates the characteristic unidirectional anisotropy and negative exchange bias field. In this approximation, the magnetic structure of the AFM phase remains unchanged during the magnetization reversal process. From (1), the equilibrium angles of magnetization can be easily calculated for $\alpha \sim 0$ and $m_{AFM} \sim 0$, and the exchange bias field can be obtained: $H_{EB} = -J_{EX}/(m_{FM}V_{FM})$.

As the real interfaces are far away to the ideal sharp AFM/FM interface, the predicted H_{EB} value is overestimated even by several orders of magnitude. Novel

experimental and theoretical approaches show the presence of pinned and unpinned spins at the interface, where only the AFM pinned spins, exchange coupled with the FM phase, give place to the loop shift after the field cool process. As a consequence, the coupling energy should be normalized by replacing it by an effective J_{EFF} value that accounts for the pinned spins faction ρ, $J_{EFF} = \rho J_{EX}$, which reduces the surface exchange energy consistently with the smaller H_{EB} observed [3, 49, 53]. Ohldag and co-workers [49, 40], from X-ray circular dichroism experiments on exchange bias multilayers, found that only a small fraction of interfacial spins ~4% is pinned to the AFM component. Similar results were reported in several core/shell systems as Fe@Cr [3], MnO@Mn_3O_4 [53, 67], Fe/γ-Fe_2O_3 [21], CoO@$Co_{1-x}Zn_xFe_2O_4$ [29]where the strength of the exchange coupling is correlated with the density of interfacial frozen spins. The exchange bias shift is often accompanied by a vertical shift displacement of the magnetization loop originated by the uncompensated AFM spins that remain pinned during the hysteresis loop. Size dependence studies show that the vertical shift, which is proportional to the number of pinned spins, has a non-monotonous dependence with the size as shown in Fig. 4.3 for the Fe/γ-Fe_3O_4

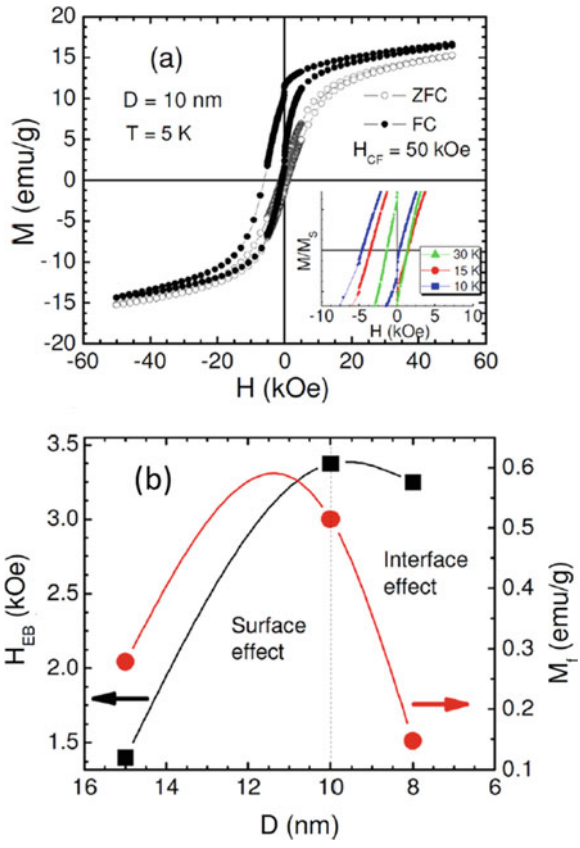

Fig. 4.3 **a** Zero-field cooling (ZFC) and field cooling (FC) magnetization loops taken at $T = 5$ K for 10 nm Fe/γ-Fe_2O_3 nanoparticles. The inset shows the FC $M(H)$ curves at different temperatures. **b**Exchange bias field (H_{EB}) and the net magnetic moment of the frozen spins (M_f) plotted as a function of particle. Reprinted from Khurshid et al. [21], with the permission of AIP Publishing

system [21]. However, although these quantities are related, the observation of a H_{EB} does not necessarily require the existence of uncompensated AFM spins.

Notice that the expression obtained for the exchange bias, within these approximation, does not depend on the magnetic anisotropy neither the size of the AFM phase. However, experimental evidence [41] shows that an AFM size threshold should be overcome to observe an exchange bias field. Figure 4.4 shows the dependence of $\mathbf{H_{EB}}$ of Fe_3O_4(FiM)core/CoO (AFM) shell nanoparticles as a function of the AFM shell thickness, where a non-monotonous dependence of the H_{EB} with the thickness is observed [38]. These results could be understood in terms of the diminution of the AFM anisotropy when the size of the AFM component diminishes beyond a critical thickness and, as a consequence, the AFM component is not longer pinned during the

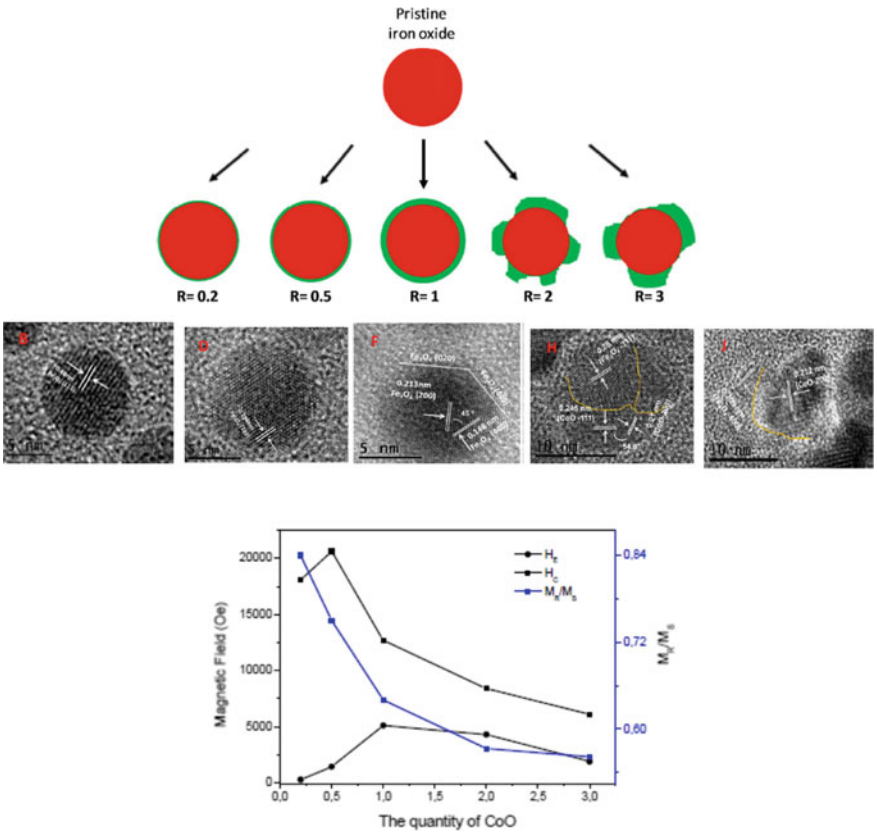

Fig. 4.4 Schematic and TEM image of the $Fe_{3-\delta}O_4$@CoO core/shell nanoparticles. The drawing shows the profile sections as a function of the Co(stearate)$_2$/Fe(stearate)$_2$ molar ratio *R*. $Fe_{3-\delta}O_4$ in red and CoO in green. The bottom graph shows the exchange bias field (H_E, ●) and the coercive field (H_C, ■), after FC and squareness (M_R/M_S, Bluebox) obtained from M(H) curves and plotted as a function of *R*. Adapted with permission from Liu et al. [38]. Copyright (2015) American Chemical Society

magnetization reversal mechanism. In spite of this, the authors call the attention on the complexity of the system that should be taken into account to interpret the results. On one hand, the growth process leads to a homogeneous CoO shell formation when the coating is thin, while polycrystalline discontinuous shell is found for thicker thicknesses. On the other hand, interdiffusion at the interface was found which leads a $CoFe_2O_4$ thin layer formation to be observed, only, in the thinner CoO shell. The presence of this hard/soft interface could result in the huge coercivity increase and the diminution of the exchange bias for the lower Co concentration.

Another parameter that plays a fundamental role in the exchange bias strength is the lattice mismatch between core and the shell phases. Depending of the system, different effects were reported. In the size dependence of Co-core/Co_3O_4-shell nanoparticles study it was found that the exchange bias field and the vertical shift present a maximum when the lattice mismatch is maximized. This result is associated with the increase of the interfacial magnetic anisotropy with the strain $\varepsilon_{Co} = (a_{Co} - a_{Co\text{-}bulk})/a_{Co\text{-}bulk}$, and also it is related with the increase of pinned spins with the lattice mismatch [8, 26, 51]. On the contrary, when the Co-core/CoO-shell nanoparticles are embedded in Cu_xO matrix, the exchange bias and the coercivity was optimized by diminishing the mismatch between the AFM shell and the matrix. In this case, by diminishing the mismatch, the highly anisotropic CoO phase is stabilized and also an increase of the number of pinned and unpinned uncompensated spins as a consequence of the interdiffusion of the Cu ions into the CoO shell is observed. This strategy could be reaches by modulating the oxygen partial pressure and therefore adjusting the Cu_xO phases, been Cu, Cu_2O, Cu_4O_3 or CuO, of the matrix [17]. These examples illustrate different approaches to maximize the anisotropy of the AFM phase and as a consequence optimize the EB effects.

Most of the researches on core/shell exchange bias systems report ferromagnetic coupling at the interface which is compatible with the negative H_{EB} usually observed. Different couplings were evaluated mainly from Monte Carlo simulations, however, only recently could be experimentally detected. Bimagnetic core/shell nanoparticles based on iron and manganese oxide were studied, and antiparallel coupling at the interface was found with the corresponding positive exchange bias field [11]. Interestingly, it was proved that the sign and the magnitude of the exchange bias field can be controlled by the cooling field, which give an additional tool to handle the EB effect.

Up to here we have discussed the reversal process when the AFM anisotropy energy is larger than the interface exchange energy, in the opposite situation: $J_{EX} \gg K_{AFM} V_{AFM}$, the AFM and FM phases are rigidly coupled and an enhancement of the magnetic anisotropy with the consequent coercivity increase is observed. From the equilibrium condition of the free energy, in the approximation $\alpha \sim \beta$ the coercivity field can be estimated:

$$H_C = \frac{2(K_{FM} V_{FM} + K_{AFM} V_{AFM})}{m_{FM} V_{FM} + m_{AFM} V_{AFM}},$$

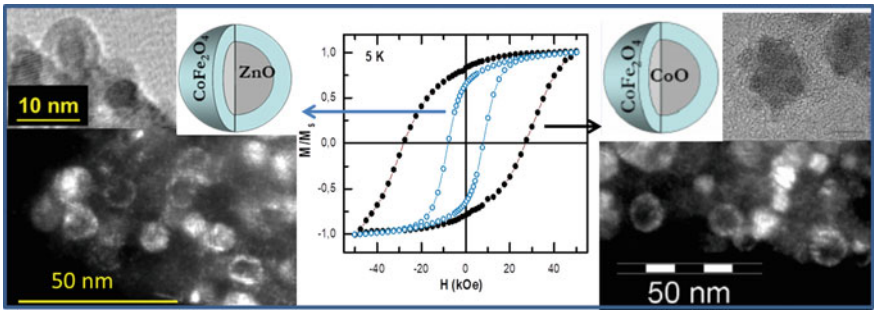

Fig. 4.5 TEM image of $ZnO/CoFe_2O_4$ and $CoO/CoFe_2O_4$ core/shell nanoparticles and the corresponding magnetization loops measured at $T = 5$ K, where the increase of the coercive field by the interface exchange coupled in the second sample is remarkable

where H_C results an average of the magnetic parameter of both phases. Figure 4.5 illustrates the coercivity enhancement by the interface exchange coupling observed in core/shell nanoparticles of 7.4 nm mean diameter [62]. In the figure, the magnetization loop of $CoFe_2O_4$ ferrite is compared when it grows over a diamagnetic ZnO or an AFM CoO core. In the former case, the coercivity result 7.8 kOe, instead in the exchange coupled $CoFe_2O_4/CoO$ system H_C increase more that 300% reaching the 27.8 kOe evidencing the magnetic hardening of the nanostructure by the interfacial exchange interaction.

The intrinsic complexity of core/shell nanoparticles makes it difficult the analysis of the exchange bias effect and the particularity of each system makes hard to including all the results in a single model. However, although the modified [43] phenomenological model fails to give a quantitative description, it provides a correct qualitative description of the systems, which results very useful for choosing suitable materials for designing nanostructures with tuned property.

4.3.2 Exchange Spring Behavior

The search of high-performance magnets has driven the development of nanostructured magnetic material that maximize the energy product $(BH)_{max}$, which can be achieved by increasing both the saturation magnetization and the coercive field. Therefore, the strategy is to combine at the nanoscale a FM (FiM) soft magnetic material, to maximize M_S, exchange coupled with a hard magnetic material, which usually presents lower M_S, to maximize H_C. This approach has the advantage of reducing the proportion of hard magnetic material based on rare earth with the corresponding cost reduction. However, as was settled by Kneller and Hawig in their pioneering work [22], when the fraction of FM soft material increases, a critical thickness, δ_c, is found. Below δ_c, both phases are rigidly exchange coupled and switch their magnetization simultaneously, whereas for larger thicknesses, the soft

phase nucleates and rotates reversibly at a lower magnetic field, as it is illustrated in Fig. 4.6. The critical thickness is related with the exchange length and results approximately twice the domain wall of the hard phase $d_H = \pi(A_H/K_H)^{1/2}$, where A_H and K_H are the exchange and anisotropy constant of the hard phase, respectively. Therefore, in hard/soft or soft/hard core/shell nanoparticles, when the thickness of the soft layer t_s is smaller than the δ_c, the magnetization of both materials is strongly coupled and invert simultaneously at a switching field H_{SW}, which results in an

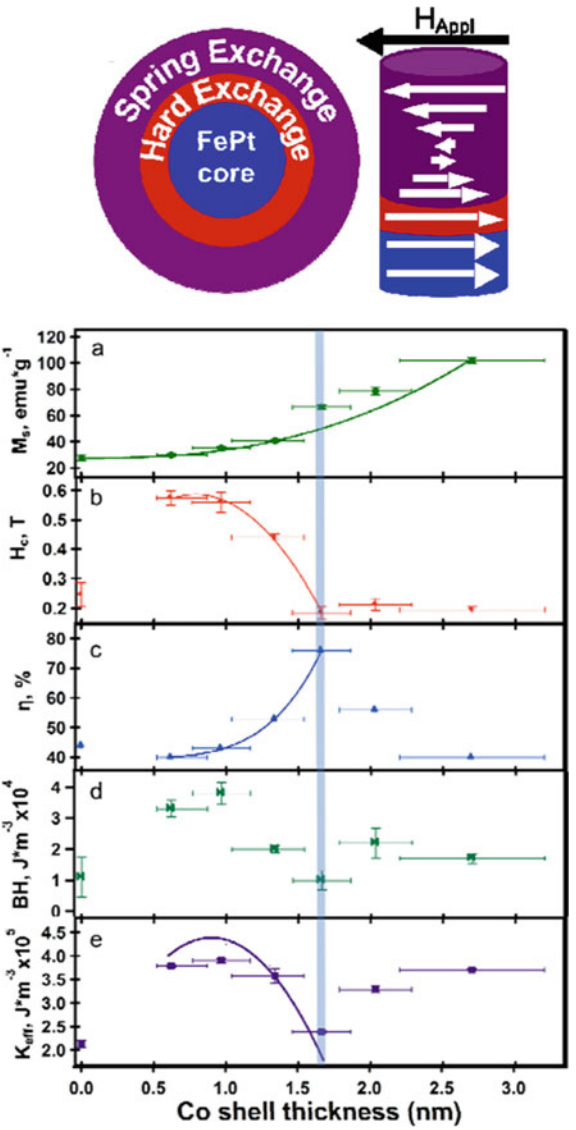

Fig. 4.6 Diagram of the proposed magnetic exchange regimes in the core/shell nanoparticles. Magnetic properties of FePt@Co nanoparticles as a function of the Co shell thickness: **a** saturation magnetization, Ms, **b** coercive field, Hc, **c** % remnant magnetization recovery, **d** energy product, BH, and **e** anisotropy constant, Keff. The blue shaded line indicates the maximum exchange-spring effect. Reprinted with permission from Carnevale et al. [4]. Copyright (2016) American Chemical Society

average of the parameters of both phases, $H_{SW} = 2(K_H V_H + K_S V_S)/(M_H V_H + M_S V_S)$, where K, M and V are the magnetic anisotropy, saturation magnetization, and volume, respectively, and the subindex S and H correspond to the soft and hard component.

When the thickness of the soft phase is larger than the critical thickness, $t_s > \delta_c$, the magnetization of both phases remains parallel until the Bloch-type domain wall nucleates in the soft phase at the magnetic field $H_N = \pi^2 AS/(2M_S tS^2)$, where A_S is the exchange constant of the soft component. For magnetic fields larger than H_N the domain wall moves toward the interface where the spins are pinned to the hard magnetic component (see Fig. 4.6). When H is further increased above H_{irr}, the domain wall will be compressed to the interface till the energy necessary for a displacement of the domain wall into the hard magnetic phase is reached. The irreversible field is usually smaller than the switching field of the hard phase but has the same order of magnitude. Below H_{irr} a reversible behavior of the magnetization is observed which resembled spring behavior, which originated the name of the process. Finally, when $t_s \gg \delta_c$ the magnetization inversion process corresponds to two independent phases.

The predicted evolution from rigid-coupled to exchange spring and beyond the exchange coupled behavior is nicely illustrated in the hard/soft $Fe_{0.65}Pt_{0.35}$-core/Co-shell nanoparticles case [4]. The system was synthesized by one-pot microwave chemical route which allows the control of the Co shell thickness from 0.6 to 2.7 nm over the hard fcc $Fe_{0.65}Pt_{0.35}$ of 5 nm of diameter. From the low-temperature hysteresis loop, the size dependence of the magnetic parameters was obtained as shown in Fig. 4.6. As expected, the saturation magnetization of the system systematically increases with the shell thickness, following a volumetric power law $M_S \propto r^3$. Conversely, the coercivity field follows non-monotonic size dependence. For a thinner Co layer, the H_C increases, a behavior ascribed to the improving of the hard magnetic properties due to the strong exchange coupling between the interface Co spins and the FePt core. When the thickness of the shell increases, the coercivity decreases due to the weaker pinning action exerted by the FePt hard magnetic phase over the outer Co layers, within this size range exchange spring process is observed. For a thicker shell, the magnetic behavior is dominated by the soft FM Co, as a consequence H_C diminishes and tends to an asymptotic value. An important consequence of the described behavior is the enhancement of the energy product which increases from 1.10(8) MGOe for FePt nanoparticles up to 3.82(5) MGOe when the core is encapsulated by a 1 nm thickness Co shell.

Finally, as the advanced chemical methods enabled to obtain monodispersed nanoparticle systems, large area of self-assembled nanoparticles can be fabricated. These systems look to optimize the core/shell nanoparticles as building blocks for advanced permanent magnetic applications reaching promising results at room temperature, as the FePt–Fe3O4 nanocomposites with an energy product of 20.1MGOe [65], FePt/Co [37], or rare-earth free core/shell nanoparticles $CoFe_2O_4/CoFe_2$ [56].

Much has been advanced in this time driven by new techniques of manufacture and characterization, and a large number of different materials has been fabricated

depending on the particular problem to be analyzed, or the magnetic response that it wanted to be achieved. In most of the cited examples, the magnetic response of bimagnetic nanoparticles is tuned by controlling the size of the core or shell components or by combining materials with different magnetocrystalline anisotropy. In the next section, we will discuss an alternative approach to control the magnetic properties as a function of the interface exchange energy.

4.4 Tuning the Magnetic Properties by the Interface Exchange Coupling

In Sect 4.3, the exchange bias effect was analyzed in AFM/FM(FiM) or FM(FiM)/AFM core/shell systems by comparing the magnetic anisotropy energy of the AFM phase with the interface exchange energy, where two limit situations were considered $K_{AFM}V_{AFM} \gg J_{EX}$ and $K_{AFM}V_{AFM} \ll J_{EX}$. Here, we present a model system to analyze the evolution of the exchange bias effect as a function of the interface coupling. With this aim CoO, AFM nanoparticles of ~3 nm of diameter were synthesized by high-temperature decomposition of organometallic precursor and encapsulated with a $Co_{1-x}Zn_xFe_2O_4$ shell of ~4 nm thickness. It is expected that by replacing the Co^{2+} ($3d^7$, $S = 3/2$) by Zn^{2+} ($3d^{10}$, $S = 0$) the strength of the interface exchange coupling would be reduced, therefore a change from rigid coupling ($K_{AFM}V_{AFM} < J_{EX}$) to exchange bias regime ($K_{AFM}V_{AFM} > J_{EX}$) could be obtained. In order to perform a systematic study, the CoO cores were synthesized in one step and split in five batches to overgrow the shells with different compositions, and this step assures that the properties of the AFM component are comparable in all the studied systems. Figure 4.7 shows TEM images of the five systems studied named Zn-x, where x corresponds to the Zn concentration that changed nominally as $x = 0, 0.25, 0.50, 0.75, 1$. All the systems present comparable size ~ 11 nm and similar morphology, also notice that the shell is formed by several nanograins in close contact as was observed in other core/shell system [36, 38].

From the FC and ZFC magnetization loops, the coercivity and the exchange bias fields were obtained and they are shown in Fig. 4.8. Also, for comparison, the field values for 8 and 5 nm $CoO/CoFe_2O_4$ core/shell bimagnetic nanoparticles [29] and the coercivity of $(Co_{1-x}Zn_x)Fe_2O_4$ single-phase nanoparticles [19, 18] are included. Several features of this figure call the attention: the coercivity field monotonically decreases with the Zn concentration, while the H_{EB} presents a maximum H_{EB} ~1500 Oe for $x = 0.25$; also, when the H_C values are compared with the obtained for the single-phase ferrite, the magnetic hardening of the system is evidenced. Moreover, it is noteworthy that H_C and H_{EB} can be systematically changed without producing a significant modification of the magnetization.

As it is known, the magnetocrystalline anisotropy is originated in the spin orbit coupling. In the cobalt ferrite, the Co^{2+} ($3d^7$, $S = 3/2$) occupy the octahedral site of the spinel structure resulting in a degenerate ground-state energy level with nonzero

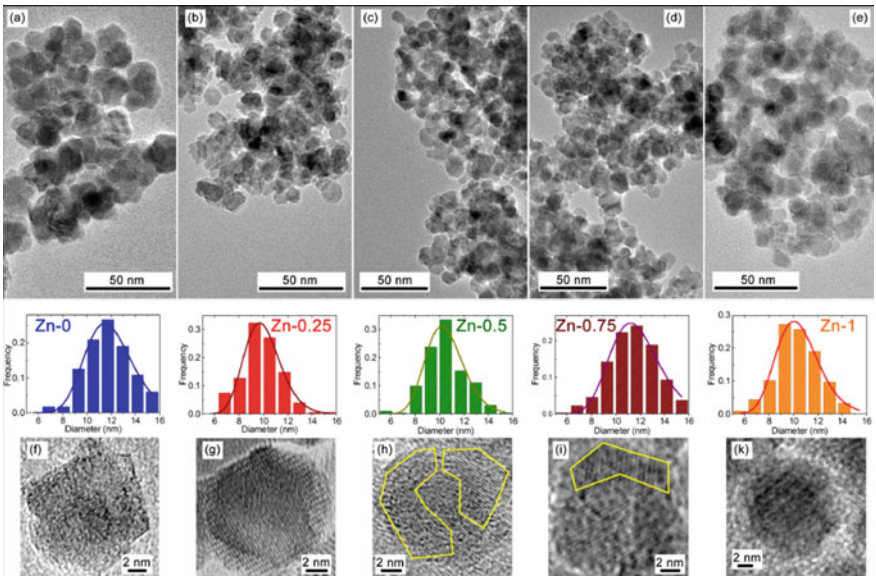

Fig. 4.7 **a–e** Transmission electron microscopy image, with the corresponding size histograms, and **f–k** high-resolution TEM images of CoO/ $Co_{1-x}Zn_xFe_2O_4$ ($x = 0$–1) core/shell nanoparticles (samples name Zn-x). Reproduced from Lavorato et al. [32] with permission from The Royal Society of Chemistry

orbital angular momentum [7, 47] (as a consequence the orbital magnetic moment interact with the spin originating large magnetocrystalline energy. The anisotropy constant reported for the Co ferrite at room temperature is K ~4 × 10^6 erg/cm^3 [46, 61]. On the contrary, the Zn^{2+} does not present spin orbit interaction because its outer configuration is fulfilled. Therefore, when the Zn concentration increases, it is expected a decrease of the effective magnetic anisotropy of the $(CoZn)Fe_2O_4$. This argument is consistent with the diminution of the coercivity observed with x, however it is not enough to explain the results because the magnitude of the H_C is more than 100% larger in the core/shell system that in the $(CoZn)Fe_2O_4$ single-phase nanoparticles of similar size. If the interface exchange coupling is considered, this interaction provides an additional source of anisotropy that explains the enhancement of H_C and also the presence of H_{EB}.

The interface coupling energy could be estimated from the experimental parameters as $E_{EX} = H_{EB}V_{FiM}M_S$, where V_{FiM} and M_S are the volume and the saturation magnetization of the ferrite. It is found that, for round nanoparticles systems of 11 nm with a core of 2.7 nm of diameter, E_{EX} vary approximately linearly with the Zn concentration from 1.5 × 10^{-13} erg for $x = 0.25$ to 0.4 × 10^{-13} erg for $x = 0$. Although for $x = 0$ no H_{EB} was observed, the coupling energy can be estimated from the linear extrapolation resulting E_{EX} ~ 2 × 10^{-13} erg, value close to the anisotropy energy of the CoO antiferromagnetic component $E_{AFM} = K_{AFM}V_{AFM}$~3.1 × 10^{-13} erg. Microscopically, this result could be interpreted from the modified Meilklejhon

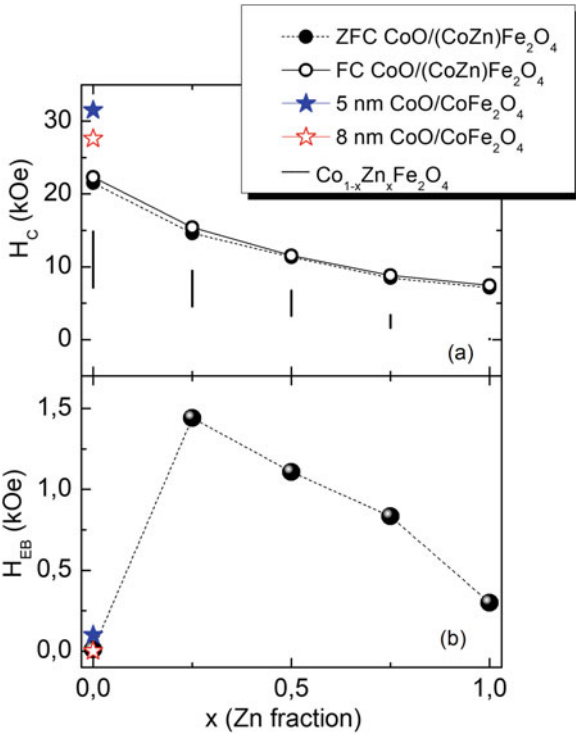

Fig. 4.8 **a** Zero-field-cooled and field-cooled (from 310 K with 10 kOe) H_C and **b** H_{EB} of $CoO/Co_{1-x}Zn_xFe_2O_4$ ($x = 0$–1) core/shell nanoparticles measured at 5 K. For comparison, the H_C of $Co_{1-x}Zn_xFe_2O_4$ [19] and [18], and also the H_C and H_{EB} values for 5 and 8 nm $CoO/CoFe_2O_4$ [29] are shown. Reproduced from Lavorato et al. [31], with permission from The Royal Society of Chemistry

and Bean model where the surface interface energy is normalized by the fraction of effective pinned spins, n, $E_{EX}/A_{int} = nJS_{FiM}S_{AFM}/a_{AFM}{}^2$, where A_{int} is the surface area, $J = J_{Co–Co} = 21.2$ K, $S_{AFM} = 3/2$, S_{FiM} is approximately 5/2, $a_{AFM} = 4.26$ Å. Figure 4.9 shows the evolution of the calculated energy and the fraction of pinned spins with the Zn concentration. The replacement of Co by the non-magnetic Zn ions induces a reduction of the interface coupling changing the relation between the involved energy E_{AFM} and E_{EX}, promoting the change of behavior from rigid coupling to exchange bias. When the Zn concentration further increases, the fraction of pinned spins continuously diminishes and the interface coupling is less effective, as a consequence the H_{EB} diminishes.

In summary, the presented approach provides a way to tune the magnetic hardening and the exchange bias field of the system by tuning the exchange coupling at the AFM/FiM interface of core/shell nanoparticles.

4.5 Future and Perspectives

The impressive advances in the physical and chemical fabrication methods have enabled the possibility to produce artificial nanostructures whose properties are

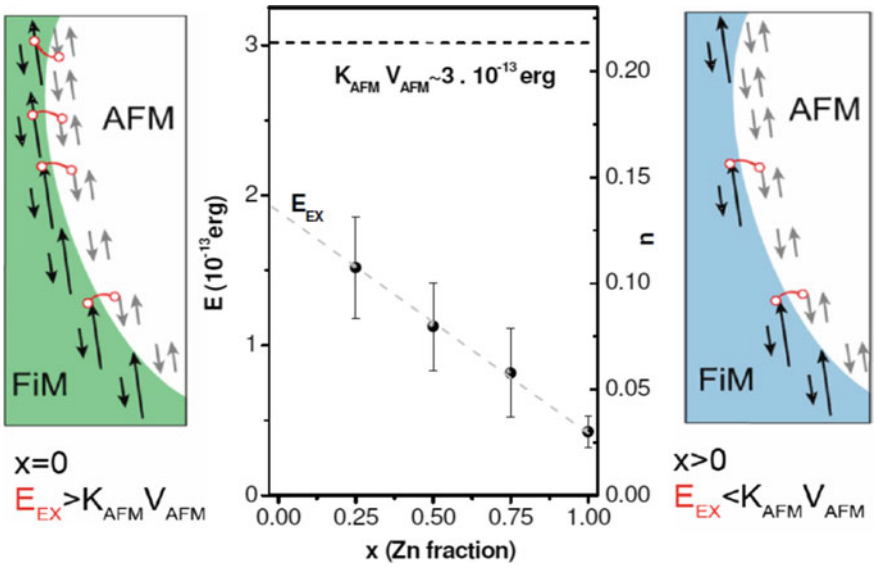

Fig. 4.9 Variation of the interface exchange coupling energy (E_{EX}) and the associated fraction of pinned uncompensated spins at the interface (n, right axis) with the Zn concentration (solid line) estimated from the experimental data (circles). The horizontal dotted line indicates the anisotropy energy of the AFM core estimated from the experimental data. The left ($x = 0$) and right ($x > 0$) panels show schematically the reduction in the effective number of exchange-coupling bonds at the interface when doping the Co ferrite with non-magnetic Zn atoms. Reproduced from Lavorato et al. [32], with permission from The Royal Society of Chemistry

different from that of their constituent materials. The core/shell nanoparticles systems have shown great versatility in the capacity to design *new materials* with tuned properties. In this chapter, we have shown that, by the interface exchange coupling, the magnetic hardening and the energy product for permanent magnets can be enhanced, and also the exchange bias can be tuned to produce an offset in the magnetization loops of great interest for spintronic and data storage applications. Recently, chemical method allows the fabrication of tunnel magnetoresistance devices based on bimagnetic nanoparticles or multicomponent superlattice [2, 6, 10, 27, 58, 60]. As it is well known, magnetic tunnel junction is composed by two ferromagnetic conducting layers separated by an insulating tunneling barrier, and the electrical resistance of the device switches between high and low resistance states as the magnetic field changes the relative orientation of the magnetizations of the two magnetic layers. In these nanostructures, the magnetic switching field is determined by the magnetic anisotropy of the system. Therefore, the possibility of combining ferromagnetic conductors with magnetic insulators in a single nanoparticle with core/shell structure would allow the manipulation the characteristic of switching field by tuning the interface exchange coupling, which would opens new and exciting possibilities to use the nanoparticles as the building blocks for new devises. The perspectives for improvement and innovation are huge, where different nanostructures can

be developed to obtaining multiple magnetotransport, or magnetoelectric responses. Different magnetic characteristics, i.e., exchange spring, exchange bias, can be tuned by choosing different hard/soft or soft/hard core/shell materials. Also, the tunnel barrier can be modulated by modifying the shell structure and composition.

The versatility and ease production of the core/shell nanostructures were also exploited in the biomedical field. For example, for magnetic fluid hyperthermia, it is necessary to tune the nanoparticles magnetic properties in order to produce the highest specific power loss for a given alternating magnetic field. Core/shell systems are the suit material to pursue this goal since, as we have showed previously, proper anisotropy and magnetization could be easily tuned by the exchange interaction [28, 34, 50]. The development of bifunctional nanoparticles also presents an exciting perspective. For example, the incorporapproximately linearly with the Zn concentrationation of optical functionalities to magnetic nanoparticles could contribute to the future development of magnetic fluid hyperthermia and its clinical application by monitoring their presence in the intracellular medium in vitro through fluorescence microscopy. In this area, we can mention the development of bifunctional $CoFe_2O_4$(core)/ZnO(shell) nanoparticles with simultaneous photoluminescence in the visible range (shell) and optimized magnetic properties (core), suited for produce AC magnetic losses for hyperthermia treatment [33], or for MRI contrast agent [61].

An important aspect that should be taken into account for biomedical applications is the biocompatibility of these nanostructures. The surface modification of the nanoparticles, or its encapsulation with a biocompatible shell, could expand the available materials in this area and its range of applications [12]. In particular, the nanoparticles can be coated with silica [52] or hydroxyapatite [44], which could improve the biocompatibility, the nanoparticle chemical stability, reduce the toxicity and also the coating could provides an ideal support for subsequent functionalizations with active organic molecules.

The challenge for the future is the development of new core/shell nanoparticles systems where the properties are fundamentally determined by the interfaces. It is a very active area where novel systems with new properties are continuously reported. It is also an interdisciplinary field, with a tremendous impact in our society, impulsed by the synergy between the advancement in the chemical and physical fabrication methods together with the technological development of new characterization tools, and with the impetus given by the huge demand for new magnetotransport and magnetoelectronic devices or innovative biomedical therapies.

References

1. W. Baaziz, B.P. Pichon, C. Lefevre, C. Ulhaq-Bouillet, J.-M. Greneche, M. Toumi, T. Mhiri, S. Bégin-ColinJ, Phys. Chem. C **117**, 11436 (2013)
2. C.T. Black, C.B. Murray, R.L. Sandstrom, S. Sun, Science **290**, 1131 (2000)
3. C. Binns, M.T. Qureshi, D. Peddis, S.H. Baker, P.B. Howes, A. Boatwright, S.A. Cavill, S.S. Dhesi, L. Lari, R. Kröger, S. Langridge, Nano Lett. **13**(7), 3334 (2013)
4. D.J. Carnevale, M. Shatruk, G.F. Strouse, Chem. Mater. **28**(15), 5480 (2016)

5. S. Chandra, H. Khurshid, W. Li, G.C. Hadjipanayis, M.H. Phan, H. Srikanth, Phys. Rev. B Condens. Matter **86**, 014426 (2012)
6. J. Chen, X. Ye, J.O. Soong, J.M. Kikkawa, C.R. Kagan, C.B. Murray, ACS Nano **7**, 1478 (2013)
7. S.O. Chikazumi, S.H. Charap, *Physics of Magnetism* (Wiley, New York, 1964)
8. D. De, O. Iglesias, S. Majumdar, S. Giri, Phys. Rev. B **94**, 184410 (2016)
9. A. Dobrynin, D. Ievlev, K. Temst, P. Lievens, J. Margueritat, J. Gonzalo, C.N. Afonso, S. Zhou, A. Vantomme, E. Piscopiello, G. Van Tendelloo, Appl. Phys. Lett. **87**, 012501 (2005)
10. A. Dong, J. Chen, P.M. Vora, J.M. Kikkawa, C.B. Murray, Nature **466**, 474 (2010)
11. M. Estrader, A. López-Ortega, S. Estradé, I.V. Golosovsky, G. Salazar-Alvarez, M. Vasilakaki, K.N. Trohidou, M. Varela, D.C. Stanley, M. Sinko, M.J. Pechan, D.J. Keavney, F. Peiró, S. Suriñach, M.D. Baró, J. Nogués, Nature Commun. **4**, 2960 (2013)
12. S. Foglia, M. Ledda, D. Fioretti, G. Iucci, M. Papi, G. Capellini, M. Grazia Lolli, S. Grimaldi, M. Rinaldi, A. Lisi, Sci. Rep. **7**, 46513 (2017)
13. N. Fukamachi, N. Tezuka, S. Sugimoto, J. Jpn. Inst. Met. **74**, 345 (2010)
14. E.E. Fullerton, J.S. Jiang, S.D. Bader, J. Magn. Magn. Mater. **200**, 392 (1999)
15. R. Ghosh Chaudhuri, S. Paria, Chem. Rev. **112**, 2373 (2012)
16. J.A. Gomes, M.H. Sousa, F.A. Tourinho, R. Aquino, G.J. da Silva, J. Depeyrot, E. Dubois, R. Perzynski, J. Phys. Chem. C **112**, 6220 (2008)
17. J. A. Gonzalez, J. P. Andrés, R. López Antón, J. A. De Toro, P. S. Normile, P. Muñiz, J. M. Riveiro, J. Nogués, Chem. Mater. **29**, 5200 (2017)
18. F. Gozuak, Y. Köseoglu, A. Baykal, H. Kavas, J. Magn. Magn. Mater. **321**, 2170 (2009)
19. H. Huang, Y. Zhang, Z. Huang, Z. Kou, X. Yuan, Z. Ren, Y. Zhai, J. Du, H. Zhai, J. Appl. Phys. **117**, 17E711 (2015)
20. J. Jin, X. Sun, M. Wang, Z.L. Ding, Y.Q. Ma, J. Nanopart. Res. **18**, 383 (2016)
21. H. Khurshid, M.-H. Phan, P. Mukherje, H. Srikanth, Appl. Phys. Lett. **104**, 072407 (2014)
22. E.F. Kneller, R. Hawig, IEEE Trans. Magn. **27**, 3588 (1991)
23. F. Einar Kruisa, H. Fissana, A. Peleda, J. Aerosol Sci. **29**, 511 (1998)
24. K.L. Krycka, J. Borchers, G. Salazar-Alvarez, A. López-Ortega, M. Estrader, S. Estrade, E. Winkler, R.D. Zysler, J. Sort, F. Peiró, M.D. Baró, C.-C. Kao, J. Nogués, ACS Nano **7**, 921 (2013)
25. M. Kiwi, J. Mag. Mag. Mat. **234**, 584 (2001)
26. Z.-A. Li, N. Fontaíña-Troitiño, A. Kovács, S. Liébana-Viñas, M. Spasova, R.E. Dunin-Borkowski, M. Müller, D. Doennig, R. Pentcheva, M. Farle, V. Salgueiriño, Sci. Rep. **5**, 7997 (2015)
27. F. Fabris, E. Lima Jr., C. Quinteros, L. Neñer, M. Granada, M. Sirena, R.D. Zysler, H.E. Troiani, V. Leborán, F. Rivadulla, E.L. Winkler, Phys. Rev. Appl. **11**, 054089 (2019)
28. F. Fabris, E. Lima, Jr., E. De Biasi, H.E. Troiani, M. Vásquez Mansilla, T.E. Torres, R. Fernández Pacheco, M. R. Ibarra, G.F. Goya, R.D. Zysler, E.L. Winkler. Nanoscale **11**, 3164 (2019b)
29. G.C. Lavorato, E. Lima Jr., D. Tobia, D. Fiorani, H.E. Troiani, R.D. Zysler, E.L. Winkler, Nanotechnology **25**, 355704 (2014)
30. G.C. Lavorato, D. Peddis, E. Lima Jr., H.E. Troiani, E. Agostinelli, D. Fiorani, R.D. Zysler, E.L. Winkler, J. Phys. Chem. C **119**, 15755 (2015)
31. G. Lavorato, E. Winkler, A. Ghirri, E. Lima Jr., D. Peddis, H.E. Troiani, D. Fiorani, E. Agostinelli, D. Rinaldi, R.D. Zysler, Phys. Rev. B **94**, 054432 (2016)
32. G.C. Lavorato, E. Lima Jr., H.E. Troiani, R.D. Zysler, E.L. Winkler, Nanoscale **9**, 10240 (2017)
33. G. Lavorato, E. Lima Jr., M. Vasquez Mansilla, H. Troiani, R. Zysler, E. Winkler, J. Phys. Chem. C **122**, 3047 (2018)
34. G.C. Lavorato, R. Das, Y. Xing, J. Robles, F. Jochen Litterst, E. Baggio-Saitovitch, M.-H. Phan, H. Srikanth, ACS Appl. Nano Mater. **3**(2), 1755–1765 (2020)
35. E. Lima Jr., E. De Biasi, M. Vasquez Mansilla, M.E. Saleta, F. Effenberg, L.M. Rossi, R. Cohen, H.R. Rechenberg, R.D. Zysler, J. Appl. Phys. **108**, 103919 (2010)
36. E. Lima Jr., E.L. Winkler, D. Tobia, H.E. Troiani, R.D. Zysler, E. Agostinelli, D. Fiorani, Chem. Mater. **24**, 512 (2012)

37. F. Liu, J. Zhu, W. Yang, Y. Dong. Y. Hou, C. Zhang, H. Yin, S. Sun, Angew. Chem. **53**, 2176 (2014)
38. X. Liu, B.P. Pichon, C. Ulhaq, C. Lefèvre, J.M. Grenèche, D. Bégin, S. Bégin-Colin, Chem. Mater. **27**, 4073 (2015)
39. A. Lopez-Ortega, M. Estrader, G. Salazar-Alvarez, A.G. Roca, J. Nogués, Phys. Rep. **553**, 1 (2015)
40. A. Lopez-Ortega, D. Tobia, E. Winkler, I. V. Golosovsky, G. Salazar-Alvarez, S. Estradé, M. Estrader, J. Sort, M. A. González, S. Suriñach, J. Arbiol, F. Peiró, R. D. Zysler, M. D. Baró, and J. Nogués. J. Am. Chem. Soc. **132**, 9398–9407 (2010). https://doi.org/10.1021/ja1021798
41. M. Lund, W. Macedo, K. Liu, J. Nogués, I. Schuller, C. Leighto, Phys. Rev. B **66**, 544221 (2002)
42. O. Masala, D. Hoffman, N. Sundaram, K. Page, T. Proffen, G. Lawes, R. Seshadri, Solid State Sci. **8**, 1015 (2006)
43. W.H. Meiklejohn, C.P. Bean, Phys. Rev. **102**, 1413 (1956)
44. S. Mondal, P. Manivasagan, S. Bharathiraja, M. Santha Moorthy, H. Hyun Kim, H. Seo, K. Dae Lee, J. Oh, Int. J. Nanomed. **12**, 8389–8410 (2017)
45. S. Mourdikoudis, K. Simeonidis, M. Angelakeris, I. Tsiaoussis, O. Kalogirou, C. Desvaux, C. Amiens, B. Chaudret, Modern. Phys. Lett. B **21**, 1161 (2007)
46. J. Nogues, J. Sort, V. Langlais, V. Skumryev, S. Suriñach, J.S. Muñoz, M.D. Baró, Phys. Rep. **422**, 65 (2005)
47. C.R. O'Handley, *Modern Magnetic Materials: Principles and Applications* (Wiley, 1999). 978-0-471-15566-9
48. K. O'Grady, L.E. Fernandez-Outon, G. Vallejo-Fernandez, J. Mag. Mag. Mat. **332**, 883 (2010)
49. H. Ohldag, A. Scholl, F. Nolting, E. Arenholz, S. Maat, A.T. Young, M. Carey, J. Stöhr, Phys. Rev. Lett. **91**, 017203 (2003)
50. V. Pilati, R. Cabreira Gomes, G. Gomide, P. Coppola, F.G. Silva, F.L.O. Paula, R. Perzynski, G.F. Goya, R. Aquino, J. Depeyrot. J. Phys. Chem. C **122**, 5, 3028–3038 (2018)
51. A. Pratt, L. Lari, O. Hovorka, A. Shah, C. Woffinden, S.P. Tear, C. Binns, R. Kröger, Nat. Mater. **13**, 26 (2014)
52. B. Sahoo, K. Sanjana P. Devi, S. Dutta, T.K. Maiti, P. Pramanik, D. Dhara, J. Colloid Inter. Sci. **431**, 31–41 (2014)
53. G. Salazar-Alvarez, J. Sort, S. Suriñach, M.D. Baró, J. Nogués, J. Am. Chem. Soc. **129**, 9102 (2007)
54. G. Salazar-Alvarez, H. Lidbaum, A. López-Ortega, M. Estrader, K. Leifer, J. Sort, S. Suriñach, M.D. Baró, J. Nogués, J. Am. Chem. Soc. **133**, 16738 (2011)
55. E. Skoropata, R.D. Desautels, C.-C. Chi, H. Ouyang, J.W. Freeland, J. van Lierop, Phys. Rev. B **89**, 024410 (2014)
56. J.M. Soares, F.A.O. Cabral, J.H. de Araújo, F.L.A. Machado, Appl. Phys. Lett. **98**, 072502 (2011)
57. Q. Song, Z.J. Zhang, J. Am. Chem. Soc. **134**, 10182 (2012)
58. S. Sun, C. Murray, D. Weller, L. Folks, A. Moser, Science **287**, 1989 (2000)
59. M. Sytnyk, R. Kirchschlager, M.I. Bodnarchuk, D. Primetzhofer, D. Kriegner, H. Enser, J. Stangl, P. Bauer, M. Voith, A.W. Hassel, F. Krumeich, F. Ludwig, A. Meingast, G. Kothleitner, M. Kovalenko, W. Heiss, Nano Lett. **13**, 586 (2013)
60. N. Taub, A. Tsukernik, G. Markovich, J. Magn. Magn. Mater. **321**, 1933 (2009)
61. N. Venkatesha, Y. Qurishi, H.S. Atreya, C. Srivastava, RSC Adv. **6**, 18843 (2016)
62. E.L. Winkler, E. Lima Jr., D. Tobia, M. Saleta, H.E. Troiani, E. Agostinelli, D. Fiorani, R.D. Zysler, Appl. Phys. Lett. **101**, 252405 (2012)
63. M. Wu, Y.D. Zhang, S. Hui, T.D. Xiao, S. Ge, W.A. Hines, J.I. Budnick, J. Appl. Phys. **92**, 491 (2002)
64. L. Xi, Z. Wang, Y. Zuo, X. Shi, Nanotechnology **22**, 045707 (2011)
65. H. Zeng, J. Li, J.P. Liu, Z.L. Wang, S. Sun, Nature **420**, 395 (2002)

66. H. Zeng, J. Li, Z.L. Wang, J.P. Liu, S. Sun, Nano Lett. **4**, 187 (2004)
67. A. López-Ortega, D. Tobia, E. Winkler, I.V. Golosovsky, G. Salazar-Alvarez, S. Estradé, M. Estrader, J. Sort, M.A. González, S. Suriñach, J. Arbiol, F. Peiró, R.D. Zysler, M.D. Baró, J. Nogués, J Am Chem Soc 132, 9398–9407 (2010). https://doi.org/10.1021/ja1021798